Reflected Sunlight Reduction and Characterization for a Deep-Space Optical Receiver Antenna (DSORA)

B. D. Clymer[1]
Ohio State University

A baffle system for the elimination of first-order specular and diffuse reflection of sunlight from the sunshade of a deep-space optical receiver telescope is presented. This baffle system consists of rings of 0.5-cm blades spaced 2.5 cm apart on the walls of 60 hexagonal sunshade tubes that combine to form the telescope sunshade. The shadows cast by the blades, walls, and rims of the tubes prevent all first-order reflections of direct sunlight from reaching the primary mirror of the telescope. A reflection model of the sunshade without baffles is also presented for comparison. Since manufacturers of absorbing surfaces do not measure data near grazing incidence, the reflection properties at anticipated angles of incidence must be characterized. A description of reflection from matte surfaces in terms of bidirectional reflection distribution function (BRDF) is presented along with a discussion of measuring BRDF near grazing incidence.

I. Introduction

A deep-space optical communications network is currently being designed with terrestrial receiving stations [1]. Laser communication between deep-space probes and Earth stations has several advantages over radio frequency (rf) communication, including higher link capacity due to higher antenna gain (smaller divergence angle), smaller and lighter transmitter and receiver components, and lower power requirements. The receiving stations for the optical deep-space network presented in [1] are Cassegrain-type telescopes, each with primary mirrors composed of 60 hexagonal segments.

A deep-space optical communications system is not without difficulties, however. The nature of deep-space planetary missions often requires operation of the communication link during times of solar conjunction with planets and, therefore, the optical receiver must be able to operate at times when the Earth receiving station is pointed near the Sun. To permit reception at small angles of solar elongation, a sunshade composed of a honeycomb array of

[1] This work was performed under a NASA Summer Faculty Fellowship at the Jet Propulsion Laboratory, Communications Systems Research Section, Optical Communications Group. The JPL contact for author correspondence is James Lesh.

hexagonally shaped tubes has been developed [2–4]. The walls separating different tube chambers align with the gaps between hexagonal segments in the primary mirror so that obscuration of the telescope for signal reception is not increased. The dimensions of the sunshade tubes are chosen so that direct sunlight is blocked from reaching the primary mirror when solar elongation angles are larger than 12 deg.

Although the walls of the sunshade are given a black-matte finish to absorb sunlight, the surfaces still reflect 0.1–1.0 percent of incident light [5]. Because the incident sunlight can be very intense, even major reduction by absorption permits an appreciable level of stray light reflected from the sunshade walls and primary mirror to be detected along with the communication signal. High data rates for communication require low levels of background light at the detector. Therefore, a baffle system has been designed to block the first-order reflection of direct sunlight from the sunshade walls and keep it from reaching primary mirror segments. This design blocks both specular and diffuse reflections of direct sunlight for solar elongation angles greater than 12 deg. Blue sky scattered light is relatively unaffected and is left to be filtered by other means [6].

There are several constraints on the implementation of a baffle system for the reduction of stray light. Ideally, the baffles should not appreciably increase the obscuration of the telescope. Therefore, the distance that the baffle blades extend from the sunshade walls should be small. In the design presented here, blade lengths are limited to 0.5 cm to match the separation between primary mirror segments so telescope obscuration is not increased. This 0.5-cm length results in spacings of 2.5 cm between blade rings or, for a nominal sunshade tube height of 5 m, a requirement of 200 baffle rings. Because the expense of manufacturing 60 hexagonal sunshade tubes with 200 baffle rings each is appreciable, a method of estimating the improvement provided by the baffle system is desirable. For this reason, a model of the reflection of sunlight from the sunshade without baffles is required.

In the remainder of this article, a baffle system designed to block first-order reflection of sunlight is presented with specific design requirements set out in Section II. The reflection properties of black-matte surfaces in terms of bidirectional reflection distribution function (BRDF) and detected stray sunlight from the sunshade walls is presented in Section III. The measurement of BRDF near grazing incidence is presented in Section IV, and concluding remarks are given in Section V.

II. Baffle System Design

Baffle systems have been widely used to reduce stray light from the walls of telescopes [7]. A baffle system designed to prevent first-order specular reflections from reaching the primary mirror of the deep-space optical receiver antenna (DSORA) telescope is shown in Fig. 1. The separation between baffle blades results in a shadow-casting structure described as

$$\Delta h = \frac{hb}{w} \tag{1}$$

where h is height of the tube, w is the distance to the opposite wall of the hexagonal tube, and b is the length of a baffle blade. This geometry was chosen to keep the baffle blade lengths identical as well as small, so that obscuration of the primary mirror by the baffle blades is minimized. If

$$2b + t \leq s \tag{2}$$

where t is the thickness of the tube wall and s is the width of the spacing between hexagonal primary mirror segments, the baffle system presents no obscuration to the primary mirror when the telescope is pointed directly at the spacecraft. The baffle system is symmetrical about the midpoint along the height of each tube.

To show that the spacing between blades is constant for a given height and width of the sunshade tube, let z be the height of a reflection point for the ray shown in Fig. 2 with l_1 and l_2, as shown in this figure. Lines ABC and CDE define the shadow regions on the tube wall and bottom aperture that block light from reaching the primary mirror. By similar triangles

$$\frac{l_1}{b} = \frac{h - z}{w} \tag{3}$$

and

$$\frac{l_2}{b} = \frac{z}{w} \tag{4}$$

the spacing between blades is given as

$$l_1 + l_2 = b\left(\frac{h - z}{w} + \frac{z}{w}\right) = \frac{bh}{w} \tag{5}$$

Direct sunlight incident on the sunshade walls at angles greater than $\theta_{h/2}$ is restricted to the top half of the tube by the shadow defined by the top edge of the tube, as shown in Fig. 3. Specular reflections are blocked by the opposite wall, as shown by ray FGHI in the figure. Since the coating

on the wall absorbs 99 to 99.9 percent of the incident light at each reflection, light reflected from the second bounce is reduced 4 to 6 orders of magnitude below the incident sunlight intensity. Diffuse light is blocked by the shadow of the lower blade, as shown by the shaded area in Fig. 3. The tube wall between the upper blade and point H is always in the shadow of the top rim of the tube and the upper blade, so no reflection occurs in this region.

Direct sunlight rays incident on the sunshade walls at angles less than $\theta_{h/2}$ may reflect from either the top or bottom half of the sunshade tube. Figure 4 represents light reflections at angles less than $\theta_{h/2}$. Specular reflections are blocked from reaching the primary mirror as shown by ray JKLM and diffuse reflections are blocked by the shadow of the lower blade. Again, the region between the upper blade and K is always in the shadow of the top rim of the tube and the upper blade.

III. Reflection Properties of Matte Surfaces

To quantify the reflected sunlight that reaches the primary mirror if no baffle system is used, the interaction of light with reflecting surfaces is first defined in radiometric terms. The total radiant flux illuminating aperture S_m from a reflecting surface S_b is given as

$$\Phi_m = \int\int_{S_b} \int\int_{S_m} \frac{L_r(\theta_b) \cos\theta_b \cos\theta_m}{r_{12}^2} dS_m dS_b \quad (6)$$

where θ_b is the angle between the normal to the sunshade wall and the ray path between an arbitrary reflection point and an arbitrary point in the aperture S_m, θ_m is the angle between the normal of S_m and the ray path, and r_{12} is the length of the ray path [8]. The value Φ_m is the radiometric flux of the light through the observation aperture S_m, while L_r is the radiance of the light reflected.

Often, reflecting surfaces are characterized by their BRDF, which relates the angular reflection spectrum of a uniform surface to the angle of incident light and is defined as

$$BRDF(\theta_i, \theta_b) = L_r(\theta_b)/E_i(\theta_i) \quad (7)$$

where θ_b is the angle between the direction of observation and the surface normal and θ_i is the angle between the direction of incident light propagation and the surface normal [9]. The value $L_r(\theta_b)$ is the reflected radiance at the angle of observation, while $E_i(\theta_i)$ is the irradiance of the reflecting surface and is given by

$$E_i(\theta_i) = \Phi_i / A_b \quad (8)$$

for uniform plane wave illumination of a planar surface of area A_b. The radiometric flux at the observation aperture from Eq. (6) can be expressed in terms of the BRDF of the surface as

$$\Phi_m = \frac{\Phi_i}{A_b} \int\int_{S_b} \int\int_{S_m} \frac{BRDF(\theta_b, \theta_i) \cos\theta_b \cos\theta_m}{r_{12}^2} dS_m dS_b \quad (9)$$

for plane wave illumination of the reflecting surface.

For a given sunshade wall and a primary mirror aperture perpendicular to the wall, as shown in Fig. 5, the reflecting surface coordinates are defined as x_b and y_b for the plane $z = 0$ and the aperture coordinates are defined as x_m and z_m for the plane $y = 0$. Using this geometry, the ratio of output to input flux is given as

$$\frac{\Phi_o}{\Phi_i} = A_b^{-1} \times \int\int_{S_b} \int\int_{S_m} \frac{BRDF(\theta_i, \theta_b) y_b z_m}{\left[(x_m - x_b)^2 + y_b^2 + z_m^2\right]^2} dx_m dz_m dx_b dy_b \quad (10)$$

For rectangular illumination of a wall and a rectangular primary mirror aperture, this equation can be solved exactly in closed form for a uniform (Lambertian) BRDF using software tools such as Mathematica [10]. For non-Lambertian BRDFs and more complicated boundaries of S_b and S_m due to hexagonal apertures (or others) and associated shadow geometries, a numerical solution is required. Since BRDF data near grazing incidence are not available, they must be measured before reliable estimates of stray light reflections can be simulated.

IV. Measuring BRDF

The evaluation software for stray light in optical systems referred to in Section III generally requires information about the reflective properties of surfaces in the system. For example, lenses can have antireflection coatings that are characterized by a given BRDF, sometimes assumed to be Lambertian. These surfaces begin to become specular at angles of incidence greater than 60 deg [5]. The BRDF measurement at angles of incidence greater than 60 deg is seldom required because baffles are usually

used to handle stray-light reflections in this regime. Furthermore, near grazing incidence is difficult to measure, as will be shown in this section.

A technique for measuring the BRDF of a surface is based on the relationship shown in Eq. (9). If the dimensions of the illuminated surface S_b are small compared to r_{12} and if the dimensions of the photodetector are also small compared to r_{12}, then Eq. (9) can be approximated as

$$\Phi_m(\theta_i, \theta_m, \bar{r}_{12}) \approx \frac{\Phi_i \cos\bar{\theta}_b \cos\bar{\theta}_m A_m A_b BRDF(\theta_i, \bar{\theta}_b)}{A_b \bar{r}_{12}^2} \tag{11}$$

where $\bar{r}_{12}$ is the distance between the center of the illuminated sample region and the center of the photodetector, and $\bar{\theta}_b$ and $\bar{\theta}_m$ are the values of θ_b and θ_m, respectively, for an observation line between the centers of S_b and S_m. The maximum error in approximating $r_{12} \approx \bar{r}_{12}$ is

$$|r_{12} - \bar{r}_{12}| \leq \bar{r}_{12} \times \left(\left[1 + \left(\frac{W}{2\bar{r}_{12}\cos\theta_i} \right)^2 + \frac{W \sin\bar{\theta}_b}{\bar{r}_{12}\cos\theta_i} \right]^{1/2} - 1 \right) \tag{12}$$

where W is the diameter of the incident probe beam. The maximum error in approximating $\theta_b \approx \bar{\theta}_b$ is

$$|\theta_b - \bar{\theta}_b| \leq \bar{\theta}_b - \tan^{-1}\left(\tan\bar{\theta}_b - \frac{W}{2\bar{r}_{12}\cos\theta_i \cos\bar{\theta}_b} \right) \tag{13}$$

As long as r_{12} and θ_b are approximately constant, the BRDF can be calculated from Eq. (11) as

$$BRDF(\theta_i, \theta_b) \approx \frac{\Phi_m(\theta_i, \bar{\theta}_b)\bar{r}_{12}^2}{\Phi_i S_m \cos\bar{\theta}_b \cos\bar{\theta}_m} \tag{14}$$

If the dimensions of the illuminated reflecting surface are small, the actual area A_b becomes irrelevant. For a BRDF measurement configuration, it is desirable to maintain the detector surface normal to the line of sight, so that $\cos\bar{\theta}_m = 1$.

Estimating BRDF from Eq. (14) is straightforward. The input flux Φ_i for a given angle of incidence is controllable and can be monitored concurrently with the measurement of the flux incident on the photodetector Φ_m. The angle of observation from the reflecting surface $\bar{\theta}_b$ can be controlled by the position of the photodetector, as can the observation distance $\bar{r}_{12}$. The area of the photodetector S_m is constant. For illumination of the reflecting surface near normal incidence, dimensions of the surface are of the same order of magnitude as the dimensions of a collimated illuminating beam, making the conditions for the approximation in Eq. (11) relatively easy to meet.

Near grazing incidence, one dimension of the spot on the reflecting surface is substantially increased, as shown in Fig. 6. At $\theta_i = 85$ deg, the width of the illuminated surface is 11.5 times the width of the incident collimated beam. At $\theta_i = 87$ deg, it is 19.1 times the incident beam width, and at $\theta_i = 89$ deg, the spot width on the surface is 57.3 times the incident beam width. A trade-off exists between maximizing the detected power for a given incident light flux and minimizing the approximation errors for r_{12} and θ_b for a given probe beam flux. Lengthening $\bar{r}_{12}$ reduces the error, but also reduces the detected power for a given detector area due to beam expansion. Absorption loss at the reflecting surface of 2–3 orders of magnitude and large $\bar{r}_{12}$ requirements must be compensated by a substantial probe beam power for measurement of BRDF at near grazing incidence.

V. Conclusion

The design for a baffle system that can be used as a sunshade for a terrestrial deep-space optical receiving telescope has been presented. The system has been designed so that the baffle rings are relatively low profile and do not increase obscuration of the segmented primary mirror. Since approximately 200 baffle rings will be required in each of the 60 hexagonally shaped sunshade tubes, a basic reflection model for a sunshade without baffles has also been presented to determine cost–benefit trade-offs. Using simple geometries, an exact analysis can be performed with symbolic manipulating software to find a closed form estimate of reflected sunlight flux through the primary mirror aperture, or it may be performed numerically using more complicated geometries. The model has been presented in terms of BRDF of the surface and, therefore, a method for measuring BRDF near grazing incidence has been included.

References

[1] J. R. Lesh, "Optical Communications for Future Deep-Space Missions," submitted to *IEEE Proceedings*.

[2] E. L. Kerr, "Architectural Design of a Deep-Space Optical Reception Antenna," submitted to *Opt. Eng.*

[3] E. L. Kerr, "An Integral Sunshade for Optical Reception Antennas," *TDA Progress Report 42-95*, vol. July–September 1988, Jet Propulsion Laboratory, Pasadena, California, pp. 180–195, November 15, 1988.

[4] E. L. Kerr and C. W. DeVore, "Shutters and Slats for the Integral Sunshade of an Optical Reception Antenna," *TDA Progress Report 42-95*, vol. July–September 1988, Jet Propulsion Laboratory, Pasadena, California, pp. 196–201, November 15, 1988.

[5] S. M. Pompea, D. F. Bergener, D. W. Shepard, S. Russak, and W. L. Wolfe, "Reflectance Measurements on an Improved Optical Black for Stray Light Rejection from 0.3 to 500 Micrometers," *Opt. Eng.*, vol. 23, no. 2, pp. 149–152, March–April 1984.

[6] E. L. Kerr, "Fraunhofer Filters to Reduce Solar Background for Optical Communications," *Opt. Eng.*, vol. 28, no. 9, pp. 963–968, September 1989.

[7] W. J. Smith, *Modern Optical Engineering*, New York: McGraw-Hill, 1966.

[8] F. L. Pedrotti and L. S. Pedrotti, *Introduction to Optics*, Englewood Cliffs, NJ: Prentice-Hall, 1987.

[9] S. Manhart and R. Birkl, "Stray Light and Backscattered Light," *Proceedings of the SPIE Conference on Optical Space Communications*, vol. 1131, pp. 45–53, 1989.

[10] S. Wolfram, *Mathematica*, Redwood City, CA: Addison-Wesley, 1988.

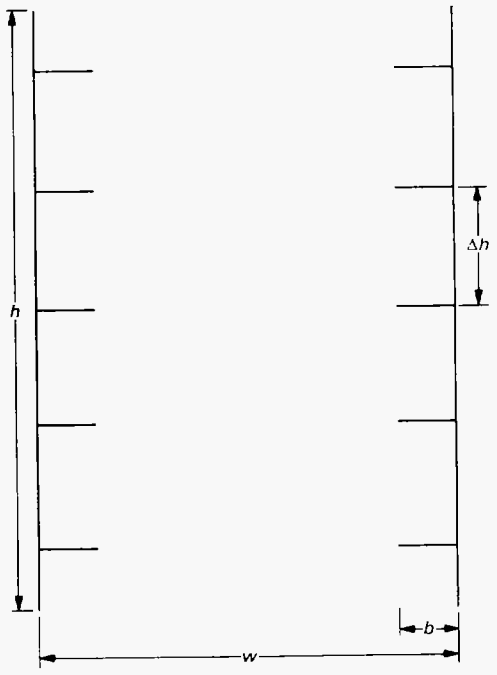

Fig. 1. Geometry for baffling to sunlight reflection from sunshade walls.

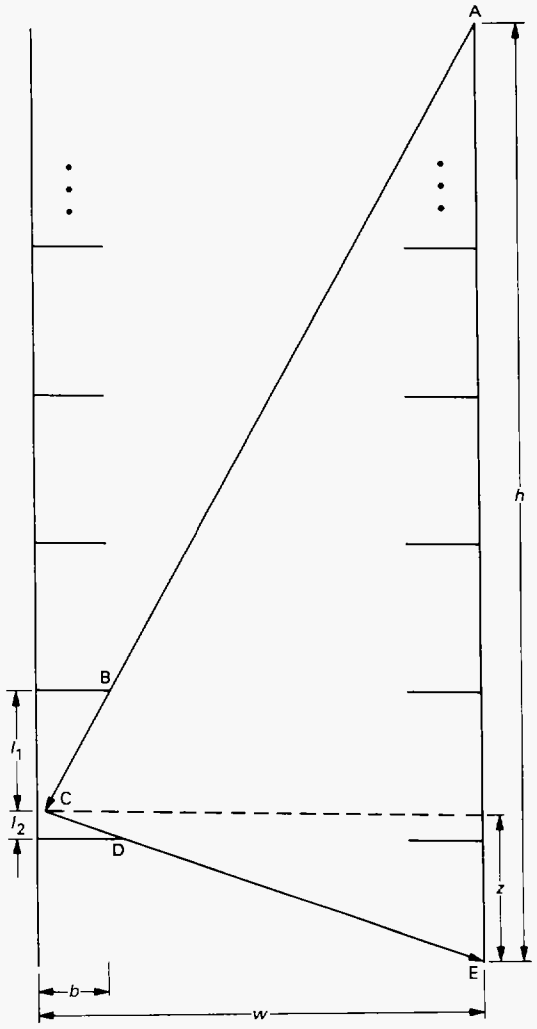

Fig. 2. Baffle spacing geometry.

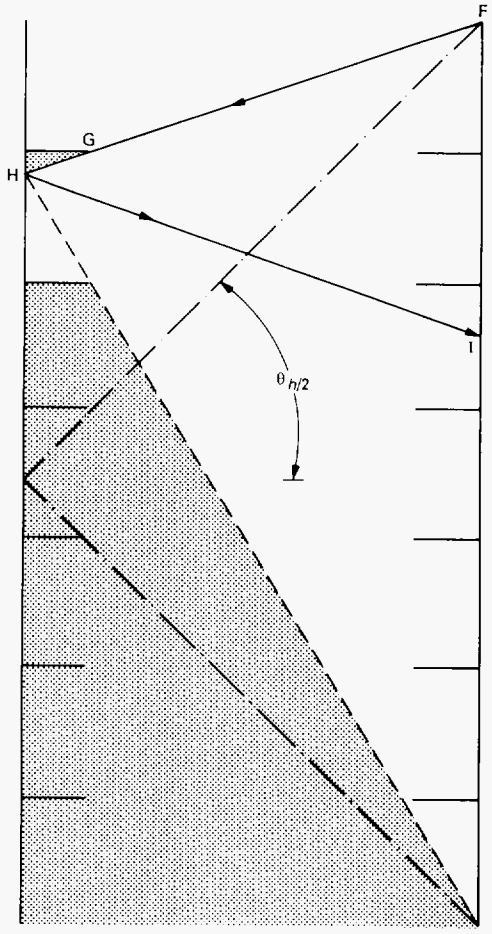

Fig. 3. Direct sunlight incident at large angles to the sunshade wall.

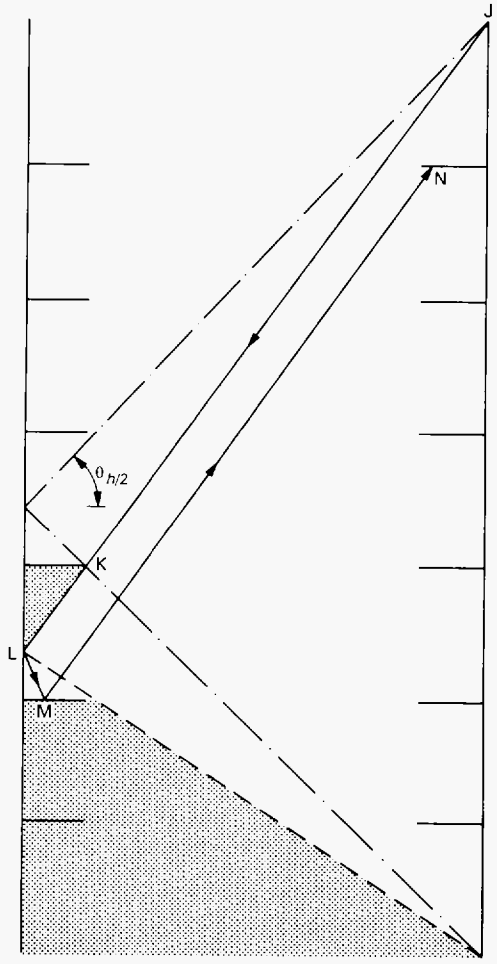

Fig. 4. Low-angle direct sunlight incidence on sunshade tube wall.

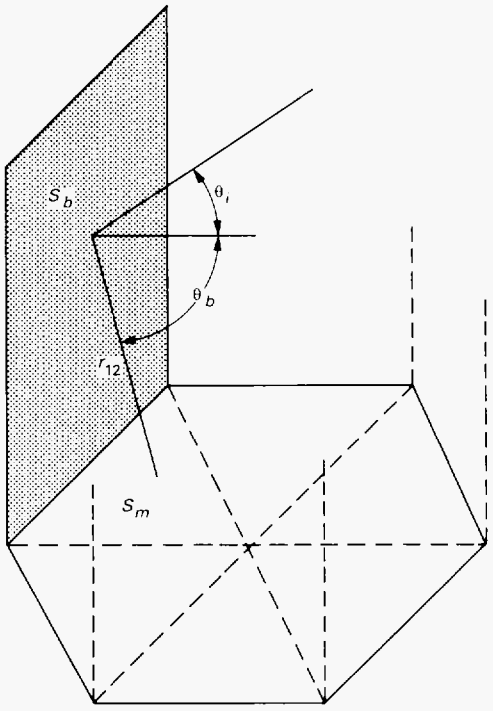

Fig. 5. Geometry for simple planar wall of the sunshade tube and perpendicular aperture.

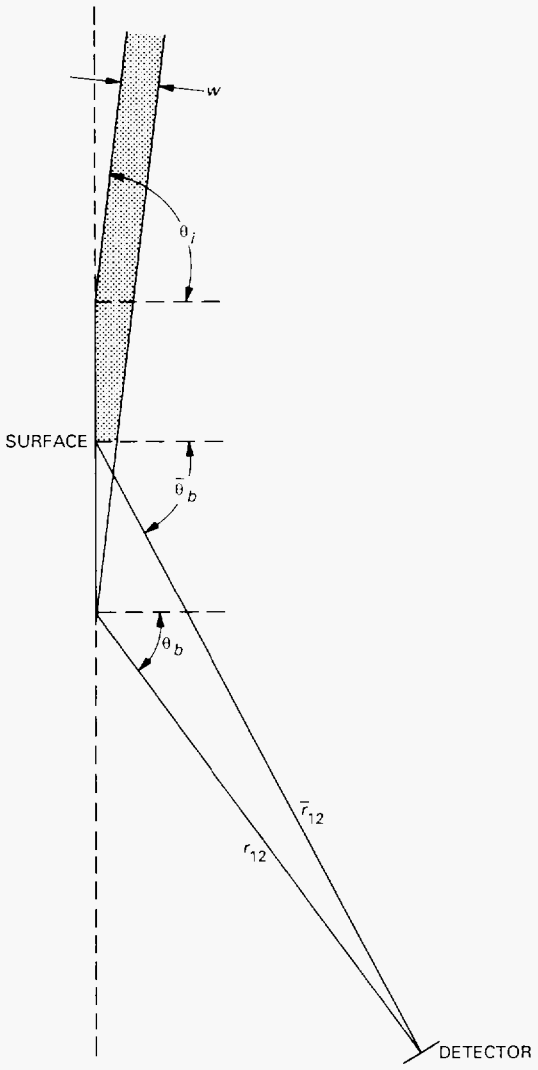

Fig. 6. Illuminated area at near grazing incidence.